NAVAL POSTGRADUATE SCHOOL

MONTEREY, CALIFORNIA

THESIS

FORMATION AND DESTRUCTION OF ARCTIC THERMOHALINE STAIRCASES

by

Kristen Ainslie

March 2021

Thesis Advisor: Timour Radko
Second Reader: Justin M. Brown

Approved for public release. Distribution is unlimited.

THIS PAGE INTENTIONALLY LEFT BLANK

REPORT DOCUMENTATION PAGE			*Form Approved OMB No. 0704-0188*

1. AGENCY USE ONLY *(Leave blank)*	**2. REPORT DATE** March 2021	**3. REPORT TYPE AND DATES COVERED** Master's thesis

4. TITLE AND SUBTITLE
FORMATION AND DESTRUCTION OF ARCTIC THERMOHALINE STAIRCASES

5. FUNDING NUMBERS

6. AUTHOR(S) Kristen Ainslie

7. PERFORMING ORGANIZATION NAME(S) AND ADDRESS(ES)
Naval Postgraduate School
Monterey, CA 93943-5000

8. PERFORMING ORGANIZATION REPORT NUMBER

9. SPONSORING / MONITORING AGENCY NAME(S) AND ADDRESS(ES)
N/A

10. SPONSORING / MONITORING AGENCY REPORT NUMBER

11. SUPPLEMENTARY NOTES The views expressed in this thesis are those of the author and do not reflect the official policy or position of the Department of Defense or the U.S. Government.

12a. DISTRIBUTION / AVAILABILITY STATEMENT
Approved for public release. Distribution is unlimited.

12b. DISTRIBUTION CODE
A

13. ABSTRACT (maximum 200 words)

This study explores the dynamics of diffusive convection, which is realized in regions where cool and fresh water-masses rest on top of those that are warm and salty. This type of convection is often observed in the Arctic Ocean and is characterized by the development of fine-scale steps in vertical salinity and temperature profiles known as thermohaline staircases. The Arctic staircases control the rate of upward heat transfer from waters of Atlantic origin, thereby influencing the melting of sea-ice and the polar climate in general. This thesis aims to utilize numerical modeling to define conditions that are favorable or unfavorable for creating thermohaline staircases and provide an explanation as to why they are not constantly prevalent throughout the Arctic. In particular, the presented high-resolution simulations explore the role of vertical shear associated with internal waves that are ubiquitous in the World Ocean. While previous investigations suggested that the vertical shear could adversely affect staircases, this effect has not been quantified and physical mechanisms at play are still poorly understood. The present study addresses these unresolved problems in the theory of double-diffusive convection, concurrently shedding light on the mechanics of heat transfer in high-latitude oceans.

14. SUBJECT TERMS thermohaline staircase, shear, double diffusion, Arctic Ocean, vertical shear, heat transfer, internal waves, convection	**15. NUMBER OF PAGES** 55
	16. PRICE CODE

17. SECURITY CLASSIFICATION OF REPORT	**18. SECURITY CLASSIFICATION OF THIS PAGE**	**19. SECURITY CLASSIFICATION OF ABSTRACT**	**20. LIMITATION OF ABSTRACT**
Unclassified	Unclassified	Unclassified	UU

NSN 7540-01-280-5500

Standard Form 298 (Rev. 2-89)
Prescribed by ANSI Std. 239-18

THIS PAGE INTENTIONALLY LEFT BLANK

Approved for public release. Distribution is unlimited.

FORMATION AND DESTRUCTION OF ARCTIC THERMOHALINE STAIRCASES

Kristen Ainslie
Lieutenant, United States Navy
BS, University of North Carolina at Chapel Hill, 2013

Submitted in partial fulfillment of the
requirements for the degree of

MASTER OF SCIENCE IN PHYSICAL OCEANOGRAPHY

from the

NAVAL POSTGRADUATE SCHOOL
March 2021

Approved by: Timour Radko
Advisor

Justin M. Brown
Second Reader

Peter C. Chu
Chair, Department of Oceanography

THIS PAGE INTENTIONALLY LEFT BLANK

ABSTRACT

This study explores the dynamics of diffusive convection, which is realized in regions where cool and fresh water-masses rest on top of those that are warm and salty. This type of convection is often observed in the Arctic Ocean and is characterized by the development of fine-scale steps in vertical salinity and temperature profiles known as thermohaline staircases. The Arctic staircases control the rate of upward heat transfer from waters of Atlantic origin, thereby influencing the melting of sea-ice and the polar climate in general. This thesis aims to utilize numerical modeling to define conditions that are favorable or unfavorable for creating thermohaline staircases and provide an explanation as to why they are not constantly prevalent throughout the Arctic. In particular, the presented high-resolution simulations explore the role of vertical shear associated with internal waves that are ubiquitous in the World Ocean. While previous investigations suggested that the vertical shear could adversely affect staircases, this effect has not been quantified and physical mechanisms at play are still poorly understood. The present study addresses these unresolved problems in the theory of double-diffusive convection, concurrently shedding light on the mechanics of heat transfer in high-latitude oceans.

THIS PAGE INTENTIONALLY LEFT BLANK

TABLE OF CONTENTS

THIS PAGE INTENTIONALLY LEFT BLANK

LIST OF FIGURES

THIS PAGE INTENTIONALLY LEFT BLANK

LIST OF TABLES

THIS PAGE INTENTIONALLY LEFT BLANK

LIST OF ACRONYMS AND ABBREVIATIONS

2D	two-dimensional
3D	three-dimensional
AW	Atlantic water
C-SALT	Caribbean-Sheets and Layers Transects
DDC	double-diffusive convection
DNS	direct numerical simulation
Pr	Prandtl number
Ri	Richardson number
Ri_D	critical Richardson number

THIS PAGE INTENTIONALLY LEFT BLANK

ACKNOWLEDGMENTS

I want to first thank my thesis advisory team. Timour, your passion for science is clear and infectious. I never thought I would be more excited to see fluid dynamics in action, or more excited to discuss thermohaline staircases and double diffusion. Justin, you are a rock star and I simply cannot say enough good things about you. I have no doubt that you will continue to succeed in all of your future endeavors. And for the rest of the thesis team, past and present, thank you for being there for me to help with coding, discuss ideas, and collectively bang our heads on these virtual machines.

For the NPS USW and METOC faculty and staff, thank you for your patience with me as I worked through the trials of starting a family, COVID, lack of childcare, and distance learning. I absolutely loved my time here and you all made this tour especially fantastic.

Finally, for my friends and family, thank you for listening to me prattle on about thermohaline staircases, layered lattes, and general fluid dynamics that I still do not fully understand. Your support is literally priceless – especially from my parents, who listened to me vent and complain about life and reminded me that I can accomplish anything I set my mind to; from my husband, Gabriel, who supported me through distance learning and childcare concerns and who was a literal shoulder to cry on; and to my daughter Juniper, who attended several fluid dynamics courses with me during virtual learning. I hope that you achieve so much more than I can ever dream of achieving.

THIS PAGE INTENTIONALLY LEFT BLANK

I. INTRODUCTION

Double-diffusive convection (DDC) plays a substantial role in the transport of heat and salt throughout the World Ocean. However, it is especially important in the Arctic, where it can increase the vertical heat transport through the halocline layer and therefore contribute to the rate of sea ice melt (Turner, 2010). Interestingly, conditions in the Arctic are rarely favorable for spontaneous establishment of double-diffusive convection. Nevertheless, common features of DDC are prevalent throughout the Arctic. The implications of Arctic heat fluxes have captured he interest of both scientists and military planners as the effects of climate change increase access to polar region. In order to understand the significance of this process in the large-scale ocean environment, we first turn to addressing the nature of double-diffusive convection at the microscale.

A. DYNAMICS OF DOUBLE DIFFUSION

Generally, double-diffusive convection exists in a stably stratified system with two quantities that contribute to buoyancy and diffuse at different rates. In the oceanic realm, these two quantities are temperature and salinity, where temperature diffusivity is nearly 100 times higher than salinity diffusivity. There are two main regimes for oceanic double-diffusive convection: salt fingers and diffusive convection.

1. Salt Fingers

The first demonstration of salt fingers was actually an inadvertent discovery by Jevons (1857), who performed an experiment in which warm sugar solute was placed on top of cold water. He observed an "interfiltration of minute, thread-like streams" that we characterize today as salt fingers (Jevons, 1857, p. 26). However, it was not until more than a century later that any focused study of double-diffusive convection began.

Stommel et al. (1956) noted that the salinity distribution in the ocean contains a significant amount of potential energy. A few years later, Stern (1960) hypothesized that the difference in molecular diffusivities of temperature and salinity could produce convective flows in the ocean. Stern described a system in which warm, dense water sat

above cold and fresh water. If a parcel of warm and salty water is vertically displaced downward, it loses its temperature excess more quickly than its salinity excess, subsequently increasing its density and drawing down more salty water from above—this process became known as salt fingering due to the thin filament structures it produces (Stern 1960). Further studies showed that the actual values of molecular diffusivities drive the size of the salt fingers—as such, most salt fingers operate on the scale of a few centimeters in the ocean (Radko, 2013).

2. Diffusive Convection

An analogous effect can be seen in the circumstance of cold and fresh water over warm and salty water. In this situation, a parcel of cold water is displaced downward into the warm water. As it descends it gains heat but retains its salinity, making it less dense than it originally was. The decrease in density causes it to reverse direction, ascend and overshoot its initial starting point. As it passes its equilibrium, it loses heat, becomes denser, and begins to sink again. Under the right circumstances, it will continue to overshoot its equilibrium and oscillate with increasing amplitude (Stern, 1960).

The history of research behind diffusive convection is significantly shorter than that of salt fingers. After Stern (1960) first discussed the effect, Turner and Stommel (1964) showed that a stable salt gradient heated from below will create a series of layers/interfaces. The source of heat driving this convection in the Arctic is the intrusion of relatively warm and salty Atlantic Water (AW). This intrusion provides the vertical stratification required for diffusive convection (see, e.g., Bebieva & Timmermans, 2017).

The conditions required for diffusive convection to occur are actually quite restrictive. Generally, diffusively stratified waters are unstable if

$$1 < R_\rho < \frac{\mathrm{Pr}+1}{\mathrm{Pr}+\tau}, \tag{1.1}$$

Where $\tau = \frac{\kappa_S^*}{\kappa_T^*}$ is the ratio between the temperature and salinity diffusivities, $\mathrm{Pr} = \frac{\nu^*}{\kappa_T^*}$ is the Prandtl number, and ν^* is the molecular viscosity. The quantity R_ρ is the local density ratio, defined as

$$R_\rho = \frac{\beta^* \frac{\partial S^*}{\partial z^*}}{\alpha^* \frac{\partial T^*}{\partial z^*}}, \tag{1.2}$$

where α^* and β^* are the coefficients of thermal expansion and haline contraction, respectively, and $\frac{\partial T^*}{\partial z^*}$ and $\frac{\partial S^*}{\partial z^*}$ are the temperature and salinity gradients, respectively. The superscript asterisks denote dimensional variables. Assuming typical values for seawater ($\tau \sim 0.01$, $\mathrm{Pr} \sim 10$), the typical range of values for diffusively unstable waters are $1 < R_\rho < 1.1$. However, density ratios in the Arctic typically fall within the interval $2 < R_\rho < 10$, meaning that most Arctic waters are diffusively stable (Radko, 2013). One notable signature that often arises because of diffusive convection is the resultant thermohaline staircase, a series of vertically stacked convective layers of uniform *T* and *S* separated by sharp interfaces producing a characteristic "staircase" profile in plots of temperature and salinity over depth. If the normal Arctic density ratios are outside the range required for diffusive convection to occur but thermohaline staircases are still present, there must be some other physical mixing phenomenon at work in order to generate these structures.

3. Thermohaline Staircases

While salt fingers and diffusive convection undoubtedly influence vertical heat transport in the World Ocean, they also have another interesting effect in their ability to form thermohaline staircases, as first demonstrated in the lab by Turner and Stommel (1964). They showed that as salt fingers drew downward, the water would form fine-scale steps in the vertical temperature and salinity profiles. This is due to a peculiar feature of DDC, which is the tendency to mix density "up-gradient." That is, double-diffusive

convection can exacerbate, rather than diffuse, small inhomogeneities in density by drawing potential energy from the unstably stratified buoyant field. As density in low-density regions decreases and in high-density regions increases, the fluid becomes unstable to convection, forming layers (Radko, 2013). This was later observed and thoroughly documented in the Caribbean-Sheets and Layers Transects (C-SALT) experiment in 1985, where strong thermohaline staircases were present in an area of over 1 million square kilometers (Schmitt et al., 1987). Fernando (1987) later experimented with thermohaline staircases within a diffusive convection regime vice a salt finger regime. He heated a salty gradient from below, thus creating a temperature differential. As time progressed, similar structures formed as in the salt finger case. The same effect can be observed via direct numerical simulations, as first demonstrated by Molemaker and Dijkstra (1997).

The most important factor of thermohaline staircases is that they are a mechanism of heat transport from the deep warmer Atlantic Water to the surface of the Arctic. However, the amount of heat flux moving through these staircases and the subsequent implications therein is still widely debated. Early laboratory work indicated that vertical heat flux was determined by temperature and salinity differences between two layers (Turner, 1965). This vertical heat flux was later parameterized by oceanographers as the "4/3 flux law." However, Kelley (1990) compiles a series of experimental results that show that heat fluxes do not perfectly adhere to this flux law. Instead, Kelley (1990) presented a different convection cell model that better accounts for this discrepancy. Later, Kwok & Untersteiner (2011) discuss that modeling Arctic ice melt would require roughly four times the heat flux through staircases than what was predicted by Kelley's new model. Kelley et al. (2003) provides a detailed summary of the research behind calculating and modeling thermal heat fluxes as well as theories of diffusive staircase formation.

B. DISTRIBUTION OF ARCTIC THERMOHALINE STAIRCASES

Despite the conditions of the Arctic being unfavorable to double-diffusive convection, thermohaline staircases are often observed throughout the Arctic. Arctic staircases were first observed and reported in by Neal et al. (1969). Since then, significant observations of Arctic staircases have been documented and summarized succinctly by

Shibley et al. (2017). Stranne et al. (2017) and Shibley et al. (2017) found that thermohaline staircases were consistently observed in the Amerasian Basin but not at all in the Eurasian Basin south of 89N (except for one outlier in the Nansen Basin) and not along boundaries near the Atlantic Water inflow. Shibley et al. (2017) calculated that 80% of the Canadian Basin profiles indicated the presence of a staircase, while only 24% of Eurasian Basin profiles indicated so.

Because of their prevalence in the ocean, and their small scale, parameterizations are needed to approximate the fluxes due to staircases for the purposes of global climate modeling. One possible reason for the lack of staircases near boundaries, as discussed by Shibley et al. (2017), is that the boundaries have higher turbulence and therefor high shear. However, there has been little research of the impacts of shear on the disruption and heat fluxes of staircases. Furthermore, little research has been done on staircase formation in the presence of critical levels of turbulence.

C. THE INFLUENCE OF SHEAR

A less understood but nevertheless important consideration for double-diffusive convection and thermohaline staircase formation or deformation is the influence of vertical shear. In the absence of atmospheric effects, deep ocean shear can result from persistent currents or internal waves, both of which are ubiquitous in the World Ocean. Shear is traditionally quantified using the Richardson number, Ri, defined dimensionally as

$$\mathrm{Ri} = \frac{N^{*2}}{\left(\frac{\partial u^*}{\partial z^*}\right)^2}, \tag{1.3}$$

where N^2 is the Brunt-Vaisala frequency defined as

$$N^{*2} = -\frac{g^*}{\rho^*}\frac{\partial \rho^*}{\partial z^*}. \tag{1.4}$$

Here, $\frac{\partial u^*}{\partial z^*}$ is the magnitude of shear, the symbol g^* is the gravitational acceleration, ρ^* is the density of seawater, and $\frac{\partial \rho^*}{\partial z^*}$ is the density gradient.

A sheared system is dynamically unstable with respect to the Kelvin–Helmholtz instability if $\mathrm{Ri} < \frac{1}{4}$. Recently, Radko (2016) discovered the thermohaline–shear instability, which can generate fluid instabilities when $\mathrm{Ri} > \frac{1}{4}$ under specific conditions of stratification. Direct numerical simulations of this instability demonstrate that vertical shear could be critical for the formation of thermohaline staircases, whereas shear had previously been thought to only disrupt staircases (Smyth & Kimura, 2007).

This thesis aims to model the role of internal wave-driven vertical shear in double-diffusive convection and to quantify the effect of shear on thermohaline staircases. We use direct numerical simulation (DNS) to model the effect of increasing unidirectional and multidirectional oscillating shear on thermohaline staircases. Furthermore, we calculate the level of shear required to ultimately disrupt the staircase. We generally find that staircase disruption occurs at the criterion for the Kelvin–Helmholtz instability. Thus, we generally attribute staircase disruption to Kelvin–Helmholtz instability. Additionally, we also modeled staircase formation via shear instabilities. We also find that weak shear in constant temperature and salinity gradients reflective of Arctic conditions can encourage the formation of layers.

The rest of this paper is arranged as follows. Section II discusses the governing equations and general modeling setup. Section III discusses the circumstances under which staircases are disrupted by shear. Section IV discusses thermohaline staircase formation via shear instabilities. Finally, Section V provides conclusions and recommendations for future work.

II. METHODS

We start with the dimensional Boussinesq equations (see Radko, 2013):

$$\begin{aligned}
\frac{\partial}{\partial t^*}\mathbf{u}^* + \mathbf{u}^* \cdot \nabla^* \mathbf{u}^* &= -\frac{\nabla^* p^*}{\rho_0^*} - g^* \frac{\rho'^*}{\rho_0^*}\mathbf{e}_z + \nu^* \nabla^{*2}\mathbf{u}^* + \mathbf{F}^*, \\
\frac{\partial}{\partial t^*}T^* + \mathbf{u}^* \cdot \nabla^* T^* &= -w^* \frac{\partial \overline{T^*}}{dz^*} + \kappa_T^* \nabla^{*2} T^*, \\
\frac{\partial}{\partial t^*}S^* + \mathbf{u}^* \cdot \nabla^* S^* &= -w^* \frac{\partial \overline{S^*}}{dz^*} + \kappa_S^* \nabla^{*2} S^*, \\
\rho'^* &= \rho_0^*(\beta^* S^* - \alpha^* T^*), \\
\nabla^* \cdot \mathbf{u}^* &= 0,
\end{aligned} \tag{2.1}$$

where $\mathbf{u}^*$ is the fluid velocity, p^* is the pressure anomaly with respect to hydrostatic pressure, T^* is the temperature perturbation with respect to the background field $\overline{T}^*$, S^* is the salinity concentration perturbation with respect to the background field $\overline{S}^*$, ρ^* is the total density, $\rho^{*\prime}$ represents the density perturbation away from the uniform reference density of seawater ρ_0^*, and $\mathbf{F}^*$ is a forcing function. The symbol $\mathbf{e}_z$ is the unit vector in the z direction, antiparallel to gravity. The gradients of the background fields, $\frac{\partial \overline{T^*}}{dz^*}$ and $\frac{\partial \overline{S^*}}{dz^*}$, are assumed constant.

Using the standard non-dimensionalization from Radko (2013), equation set 3.1 reduces to the non-dimensional:

$$
\begin{aligned}
\frac{1}{\mathrm{Pr}}\left(\frac{\partial}{\partial t}\mathbf{u}+\mathbf{u}\cdot\nabla\mathbf{u}\right) &= -\nabla p+(T-S)\mathbf{e}_z+\nabla^2\mathbf{u}+\mathbf{F},\\
\frac{\partial}{\partial t}T+\mathbf{u}\cdot\nabla T-w &= \nabla^2 T,\\
\frac{\partial}{\partial t}S+\mathbf{u}\cdot\nabla S-wR_0 &= \tau\nabla^2 S,\\
\rho' &= -(T-z)+(S-R_o z),\\
\nabla\cdot\mathbf{u} &= 0,
\end{aligned}
\tag{2.2}
$$

where R_0 is the density ratio of just the background gradients $\frac{\partial\overline{S^*}}{\partial z^*}$ and $\frac{\partial\overline{T^*}}{\partial z^*}$. Non-dimensional units are given by

$$
\begin{aligned}
[L] &= \left(\frac{\alpha^* g^*\left|\frac{\partial\overline{T}^*}{\partial z^*}\right|}{\nu^*\kappa_T^*}\right)^{-\frac{1}{4}},\\
[t] &= \frac{[L]^2}{\kappa_T^*},\\
[T] &= \left|\frac{\partial\overline{T}^*}{\partial z^*}\right|[L],\\
[S] &= \frac{\alpha^*}{\beta^*}[T],
\end{aligned}
\tag{2.3}
$$

Where $[L]\sim 0.01m$ is the spatial scale, $[t]\sim 10^3 s$ is the temporal scale, $[T]\sim 10^{-4}{}^{\circ}C$ is the temperature perturbation scale, and $[S]\sim 10^{-2}\,\mathrm{ppm}$ is the salinity perturbation scale. The non-dimensional background temperature and salinity fields are $\overline{T}=-z$, $\overline{S}=-R_0 z$.

We construct a coordinate system that moves along with a background flow, which is described by $\overline{\mathbf{u}}=\gamma(t)z\cos(\omega t)\mathbf{e}_x+\gamma'(t)z\cos(\omega t+\frac{\pi}{2})\mathbf{e}_y$, where γ is the shear magnitude, ω is the angular frequency of the shear oscillations, and γ' can either be γ or 0 to allow

for multidirectional or unidirectional shear, respectively. This necessitates the use of the following transformation to an alternate coordinate system, designated with tildes:

$$\begin{aligned} \tilde{x} &= x - \frac{\gamma z}{\omega}\sin(\omega t), \\ \tilde{y} &= y - \frac{\gamma' z}{\omega}\sin(\omega t + \frac{\pi}{2}), \\ \tilde{z} &= z, \\ \tilde{t} &= t. \end{aligned} \tag{2.4}$$

We use these to transform Equations (3.1). To ensure that the background flow satisfies our expression for $\bar{\mathbf{u}}$, we require the forcing term to take the form $\mathbf{F} = \frac{\partial}{\partial t}\left(\gamma(t) z \cos(\omega t)\mathbf{e}_x + \gamma(t)' z \cos(\omega t + \frac{\pi}{2})\mathbf{e}_y \right)$. The resulting equations are solved using a modified version of the code described in Traxler et al. (2011). This numerical model is pseudospectral and it decomposes the perturbation quantities with Fourier series in all three dimensions, which necessitates periodic boundary conditions. The code uses a modified Patterson-Orszag method to ensure incompressibility, and the time stepping is conducted with a third-order semi-implicit Adams–Bashforth/backward-differencing formula (Canuto et al., 2007; Orszag & Patterson, 1972). The nonlinear terms are calculated in physical parameter space using a three-dimensional Fourier transform.

Throughout this study, we conduct several direct numerical simulations with general parameter settings that reflect conditions in the Arctic. Generally, each DNS is configured to begin with a perfect staircase structure in density (cold and fresh over warm and salty); that is, the domain is vertically subdivided into a number of equally sized convective layers, and the total temperature, $T + \overline{T}$, and salinity, $S + \overline{S}$, within each of the layers are initially uniform with small random seed perturbations. These layers are separated by sharp interfaces that are smoothed with a boxcar filter to avoid the Gibbs phenomenon. We vary the layer height and density ratio across the simulations (see Table 1), but the size and resolution of the simulation remains constant across all DNS. Each simulation has a shear angular frequency given by $\omega = N/10$, where in these non-dimensional units $N^2 = \Pr(R_0 - 1)$.

In these simulations, we are interested in measuring the amount of shear required to destabilize a thermohaline staircase. We parameterize the shear value by the global Richardson number and we observe the critical Richardson number in which staircase destruction occurs. In terms of non-dimensional quantities, the global Richardson number is given by

$$\mathrm{Ri} = \frac{\mathrm{Pr}(1 - R_0^{-1})}{\gamma^2}. \tag{2.5}$$

The shear magnitude γ is chosen such that

$$\begin{aligned} \gamma(t) &= \gamma_0 + \gamma_r t, \\ \gamma_0 &= \sqrt{\frac{\mathrm{Pr}(R_0 - 1)}{\mathrm{Ri}_0}}, \\ \gamma_r &= \frac{\sqrt{\mathrm{Pr}(R_0 - 1)}}{t_f}\left(\frac{1}{\sqrt{\mathrm{Ri}_0}} - \frac{1}{\sqrt{\mathrm{Ri}_f}}\right), \end{aligned} \tag{2.6}$$

where $\mathrm{Ri}_0 = 1$ is the initial Richardson number of the simulation, $\mathrm{Ri}_f = 0.2$ is the final Richardson number, and $t_f = 100$ is the time at the end of the simulation.

III. STAIRCASE DESTRUCTION

To determine the critical Richardson number at which staircases are disrupted, we conducted 18 three-dimensional DNS for $\mathrm{Pr} = 10$ and $R_0 = [2,3,5]$ with between 2 and 4 layers, as tabulated in Table 1. Each experiment was initialized with a staircase at rest within a cube of side length L=200, resolved by 384 grid points in each dimension. The shear in each simulation is unidirectional $(\gamma' = 0)$ or multidirectional $(\gamma' = \gamma)$, as denoted in Table 1.

Figures 1 and 2 illustrate the typical behavior of a simulation, which in this case had $R_0 = 3$ and 3 initial layers. The initial staircase is evident in Figure 1. As the temperature and salinity diffuse across the interface, a convectively unstable layer forms due to the different rates of thermal and haline diffusion, which then leads to convection. Simultaneously, the system feels the effects of shear, which interacts with the processes in the convective layers. At early times, the forced shear is weak, but the global Richardson number gradually decreases over time as the shear increases, described by Equation (3.6). By $\mathrm{Ri} < 0.25$, the system is unstable to the Kelvin–Helmholtz instability, and the interfaces are disrupted (as seen in Figure 2). Figure 2 shows several swirls of turbulence that are also indicative of Kelvin–Helmholtz instability behavior.

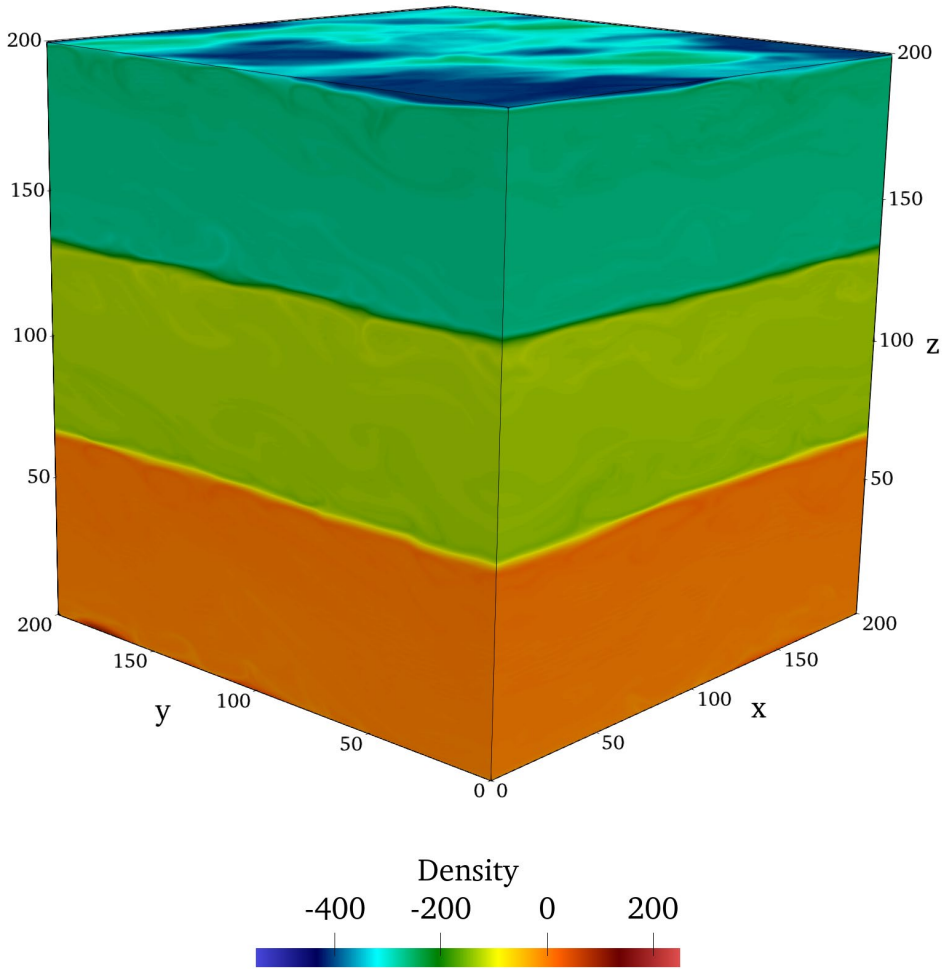

Figure 1. Initial Stage of 3D Simulation

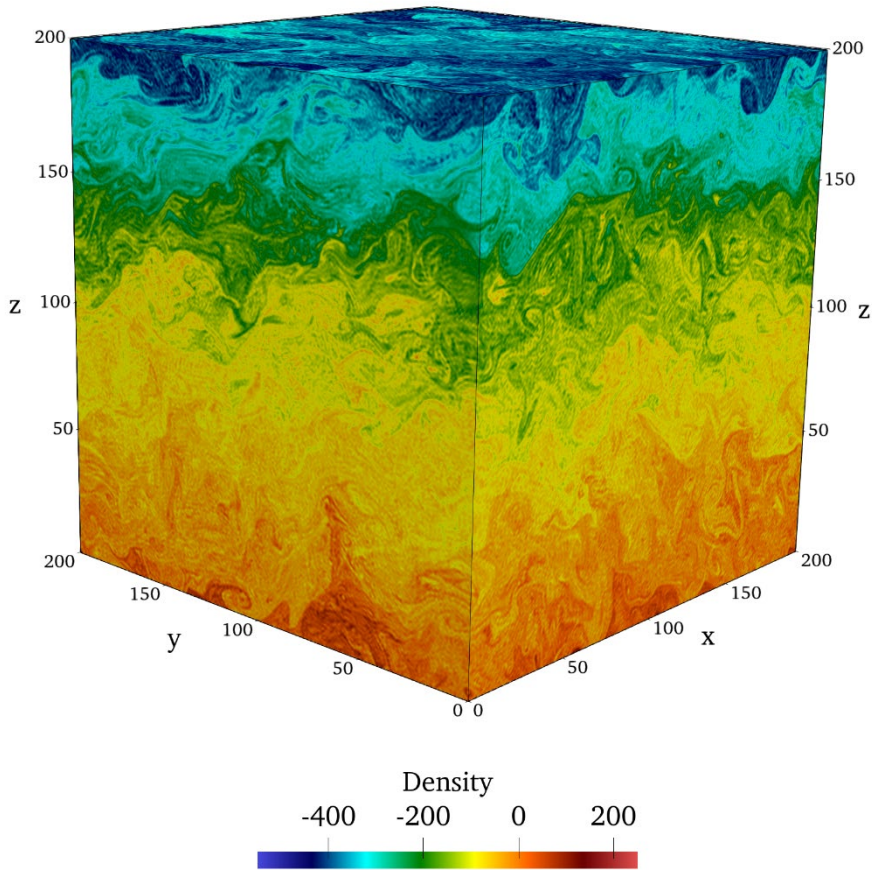

Figure 2. Final Stages of 3D Simulation

For each DNS, we estimate the non-dimensional turbulent temperature flux and the dimensional turbulent heat flux of the simulations to understand how these systems will contribute to heat transport in the ocean. We can estimate these quantities by the non-dimensional dissipation of temperature and the dimensional dissipation of heat, defined respectively as

$$F_T = \left\langle \nabla \mathrm{T}^2 \right\rangle, \tag{3.1}$$

$$F_T^* = F_T \rho_0^* c_p^*, \tag{3.2}$$

where the angled brackets indicate the spatial average over the entire domain and c_p^* is the specific heat capacity of seawater. This approximation can be justified by multiplying the temperature evolution equation by T and assuming quasi-steady equilibrium to determine

the relationship between the mean dissipation and temperature flux. The flux is then plotted as the ordinate with time and corresponding Richardson number as the abscissa in Figure 3, which shows the simulations with $R_0 = 3$. Each simulation was initialized with 2, 3, or 4 layers as indicated in the legend. Initially, the fluxes are low prior to the onset of convection, which is fully realized by $t = 20$. After this point, the fluxes reach a temporary quasi-steady equilibrium; however, as shear continues to increase, the forced shear begins to impart energy to the convection, which is evidenced by the increasing fluxes. Eventually the flux rapidly increases due to a large mixing event in all cases, which we will show is connected to staircase disruption by parametrizing the disruption time.

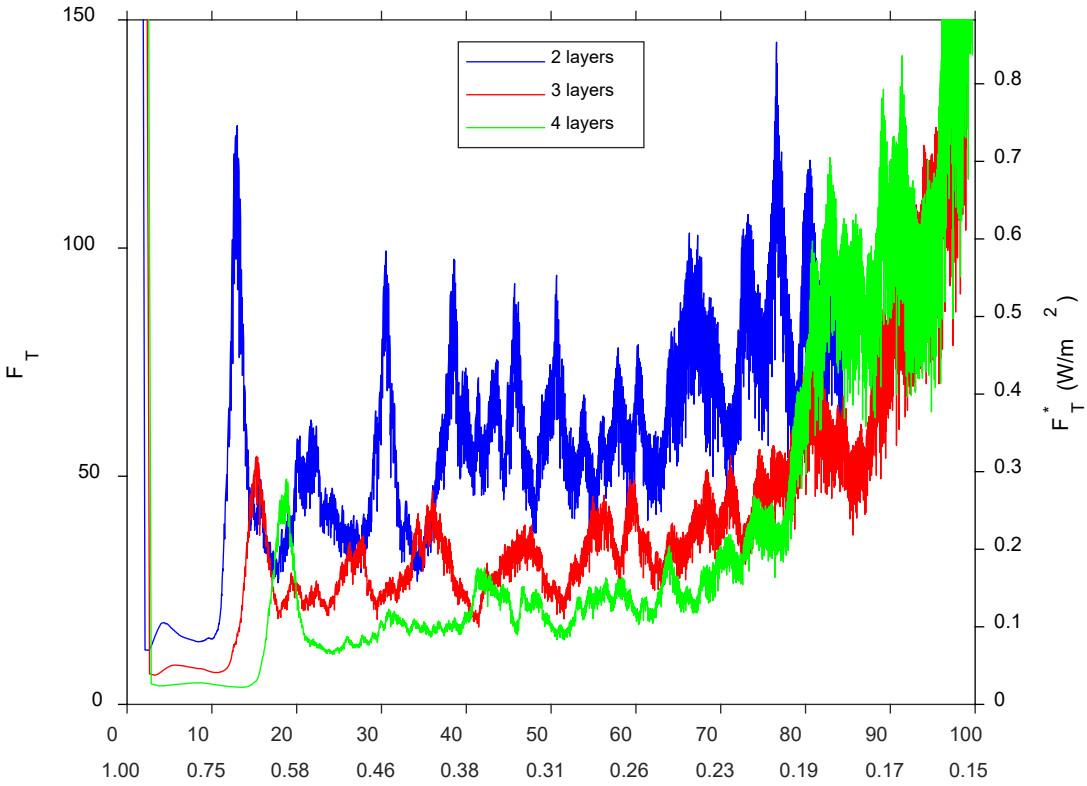

Figure 3. Heat Flux (left axis) and Turbulent Heat Flux (right axis) over Time/Richardson Number

We characterize the staircase disruption through the use of a "steppiness" parameter denoted as σ. This parameter is generated by constructing a histogram of the density for

each time, which has a value of $h(\rho_i,t)$ for the *i*th density bin, such that $\sum_{i=1}^{M} h(\rho_i,t)=1$ for all *t*, where *M* is the number of density bins (here chosen to be 400), $\rho_1=(1-R_0)L$, and $\rho_M=0$. Due to the periodic nature of the domain, any values of the density outside of this range can be brought inside it by adding or subtracting some multiple of $(R_0-1)L$, which is the constant density difference between the top and bottom of the domain. This avoids mischaracterizing fluid that has crossed the vertical boundary during the simulation. A uniform gradient density field would necessarily have $h(\rho_i,t)=\frac{1}{M}$ for all *i*. We choose to evaluate the steppiness as

$$\sigma(t)=\sum_{i=1}^{M}\begin{cases} h(\rho_i,t)\Delta\rho, \text{ if } h(\rho_i,t)>\dfrac{\delta}{M} \\ 0, \text{ otherwise} \end{cases} \tag{3.3}$$

where $\Delta\rho=\frac{(R_0^{-1})L}{M}$ is the density bin spacing and δ is an arbitrary number constrained to $\delta\geq 1$, here chosen to be 1.5 to ensure that visual inspection of a staircase shows disruption at $\sigma<0.5$. This measures the fraction of the domain that is unrepresentative of a uniform density gradient in terms of how overrepresented any particular density value is in the domain.

Figure 4 shows σ values for the 9 different multidirectional simulations grouped by density ratio. Each simulation begins with σ near 1, indicating a nearly perfectly layered density distribution. As the simulation progresses, shear continues to degrade the interfaces and subsequently, σ decreases towards 0 as the fluid becomes more uniformly distributed. Our parameterization of staircase disruption at $\sigma=0.5$ is highlighted by a red circle. 4 also highlights how staircases with smaller density ratios are more difficult to disrupt with shear, as the cases where $R_0=2$ with 3 and 4 layers were not disrupted by t=100 and the case with 2 layers only barely crosses their stepiness threshold. We can use this diagnostic to investigate the behavior of the fluxes as the staircase becomes disrupted. In 3, the fluxes rapidly increase when σ crosses below 0.5 and a large amount of material

is transported across the interfaces. Even though the time of disruption appears to correlate with the number of layers for this simulation, the precision of the steppiness parameter is not high enough to draw any systematic conclusions from this. Given the time when σ crosses this threshold, we can calculate the Richardson number at which disruption occurs, denoted by $\mathrm{Ri_D}$, also shown in Table 1. Notably, $\mathrm{Ri_D}$ increases as the density ratio increases, which indicates that less shear is required overall to disrupt the staircase. Because higher density ratios lead to a more stable system, it is more difficult to form staircases in those regions and subsequently less difficult to disrupt them.

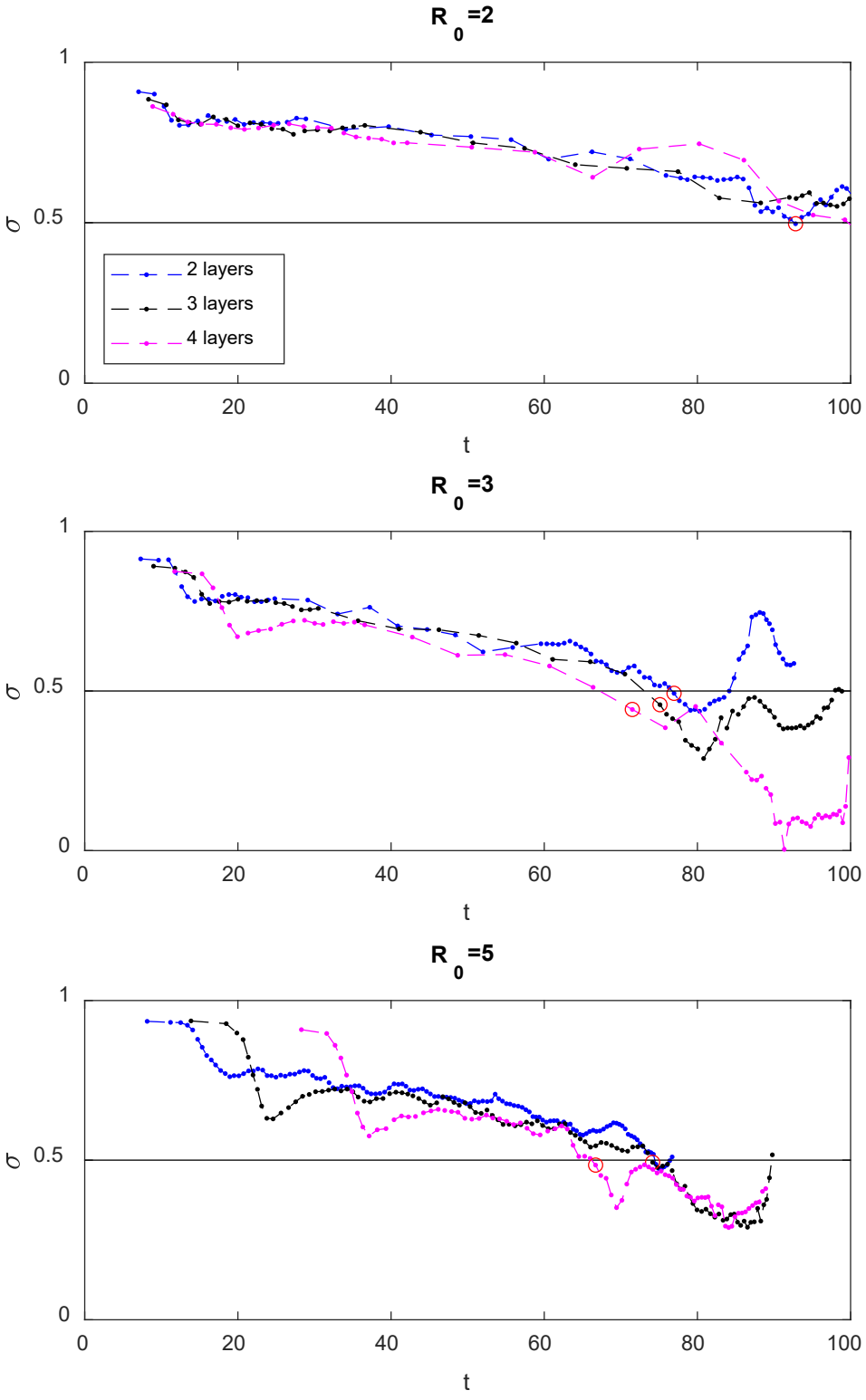

Figure 4. Steppiness (σ) Values for 9 Multidirectional Simulations

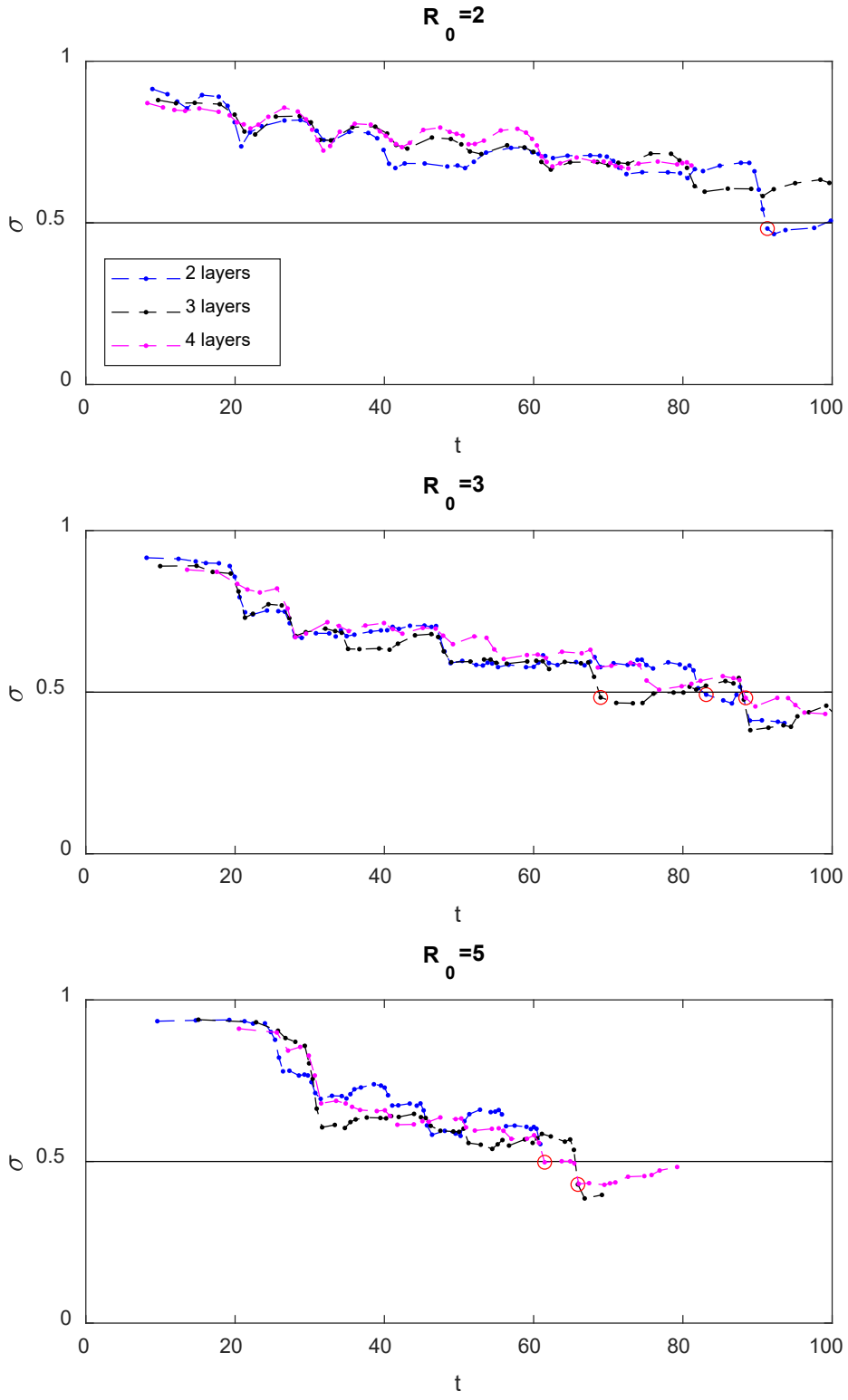

Figure 5. Steppiness (σ) Parameters for 9 Unidirectional Simulations

We also conducted a steppiness evaluation for the unidirectional shear simulations, and the results are compiled in Figure 5. However, there are no significant visual differences in the steppiness pattern for the multidirectional shear simulations as compared to the unidirectional shear simulations. If staircase disruption occurs, Ri_D is roughly between 0.16 and 0.25 for unidirectional shear while Ri_D falls between 0.15 and 0.24 in the multidirectional regime. This is consistent with the criterion for the Kelvin–Helmholtz instability. Thus, we do not see any systematic difference between unidirectional and multidirectional simulations with regards to staircase disruption. However, we do see differences in heat fluxes between the two simulations, as shown in Figure 6.

Table 1. Critical Richardson Numbers for 9 Oscillatory Simulations and 9 Rotational Simulations.

Ri_D			
	Number Layers:		
Density Ratio:	**4**	**3**	**2**
2 $\gamma_0 = 3.1623, \gamma_r = .05$	0.14995	*	0.1642
	0.1996	*	0.16745
3 $\gamma_0 = 4.4721, \gamma_r = .0707$	0.22035	0.209	0.20355
	0.1739	0.22885	0.18675
5 $\gamma_0 = 6.3246, \gamma_r = .1$	0.23685	0.2990	0.2106
	0.25715	0.23975	***

Rotational simulations are denoted by the color blue and * indicates that the staircase was not disrupted within the domain. *** in the bottom right corner indicates that the model was not completed.

Figure 6 highlights two simulations with $R_0 = 2$ and 2 initial layers. One of these simulations has multidirectional shear and the other has unidirectional shear. Both simulations begin with low heat fluxes that increase as shear increases. However, the unidirectional-shear simulation shows a strongly oscillatory heat flux at the shear frequency while the multidirectional-shear case does not. In addition, the peak fluxes for the unidirectional-shear case are significantly higher than in the multidirectional-shear case, even though they have the same minimum Richardson number. However, the mean

heat flux of the multidirectional-shear case is roughly twice that of the unidirectional-shear case. This can be explained by the magnitude of shear. The maximum multidirectional-shear magnitude does not change as the shear profile rotates, but the maximum unidirectional-shear oscillates in amplitude, the time-average of which is equal to ½ of the case with multidirectional shear. This results in the time-averaged fluxes in the multidirectional case being twice that of the unidirectional-shear case. This could have substantial implications for stochastic changes in shear direction in the ocean.

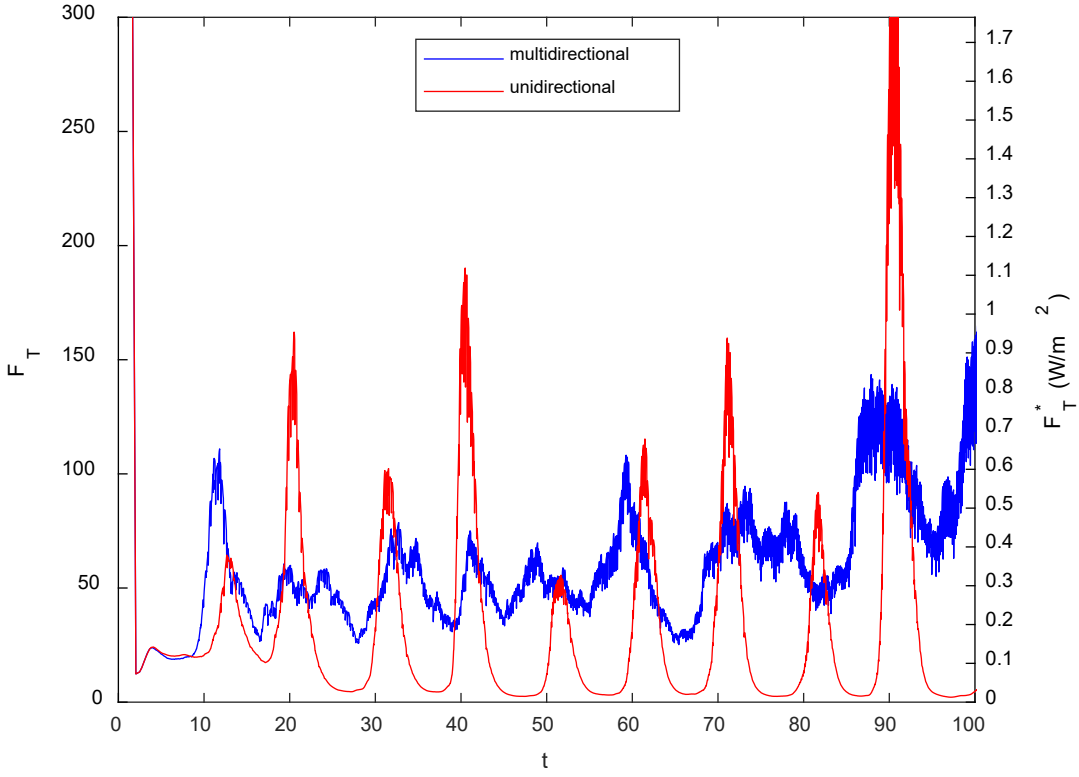

Figure 6. Multidirectional vs. Unidirectional Shear Heat Fluxes

The same simulations were replicated in 2D to highlight the disparity between two-dimensional and three-dimensional convection in the presence of shear. Due to the two-dimensional nature of the simulation, these are most comparable to the unidirectional-shear setup. The summary of the shear parameters used for each value of the density ratio in these

2D simulations is found in the first column of Table 1, and each was initialized with 2, 3, or 4 layers.

Figure 7 shows 3 snapshots in time from a simulation that was initialized with a density ratio of 5 and that initially contained 4 layers. While the behavior of double-diffusive staircases typically shows remarkably little qualitative dependence on dimensionality (see, e.g., Flanagan et al., 2013), the interaction of shear with convection demonstrates drastic differences between two-dimensional and three-dimensional simulations (see Lipps, 1971). Figure 7a shows an early stage where shear is beginning to perturb the interfaces. Generally, the two-dimensional simulations start much the same as the corresponding three-dimensional simulations, wherein the initial diffusion of temperature and salt across the interfaces leads to a development of an unstably stratified density boundary followed by convection. Figure 7b shows a stage with reasonably large shear, where the interfaces are beginning to be disrupted by a similar shear mechanism as described for 3D. After this point, the behavior deviates from the three-dimensional simulations as the increasing shear starts to weaken and eventually shut down convection. Figure 7c then shows the remaining staircase signatures decaying by molecular diffusivity. This situation occurs when modeling 2D simulations with shear.

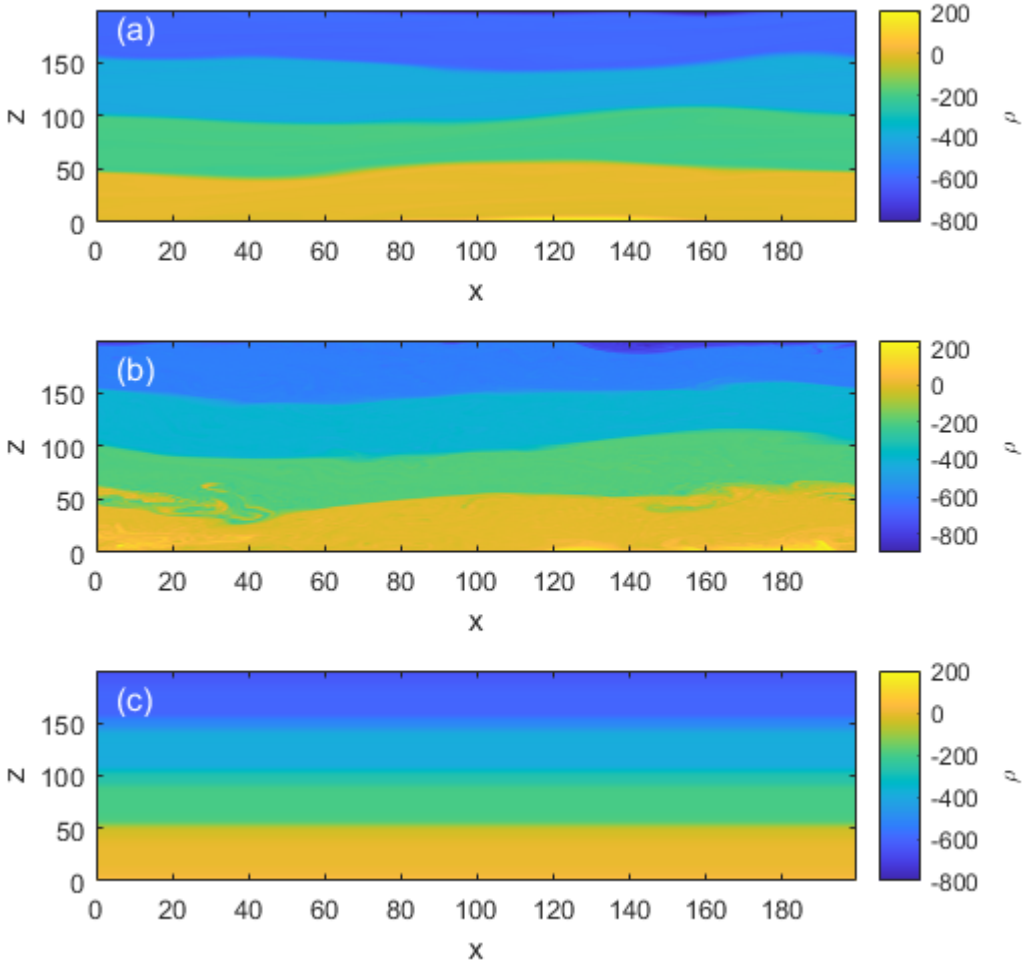

Figure 7. Density Profiles for 2D Simulations

The major difference between the two sets of simulations arises from the effect of shear; that is, shear tends to stabilize two-dimensional convection and destabilize three-dimensional convection (Lipps, 1971). Lipps (1971) described how sheared convection transports velocity up-gradient in 2D. This results in lower shear at the interface for our setup. Conversely, sheared convection transports velocity down-gradient in 3D, resulting in strong shear layers at the interface, which subsequently disrupt it. Figure 8 graphically shows the difference in the shear profiles between 2D and 3D for simulations with $R_0 = 3$ and 3 initial layers. In the three-dimensional shear profile, the shear increases dramatically at the interfaces. Conversely, while the 2D shear profile looks nearly linear, a closer examination shows that shear is slightly weaker at the interfaces. The mechanism for this

is described in Lipps (1971), shear can either serve as a source or sink for convective fluxes. In 2D, continually increasing shear results in weakening convection until it shuts down completely. At this point, the only remaining relevant mixing process is molecular diffusion. Because the thermal diffusivity is larger, the temperature field becomes a uniform gradient within a thermal dissipation time over one layer, which in our non-dimensional units is a timescale of h^2, and salinity follows after a haline dissipation time, $\frac{h^2}{\tau}$, where $h = \left(\frac{L}{n}\right)$ and n is the number of layers. Notably, this result is likely only of academic interest, as the same sort of two-dimensional shear and convection phenomena would not be realized in the three-dimensional ocean.

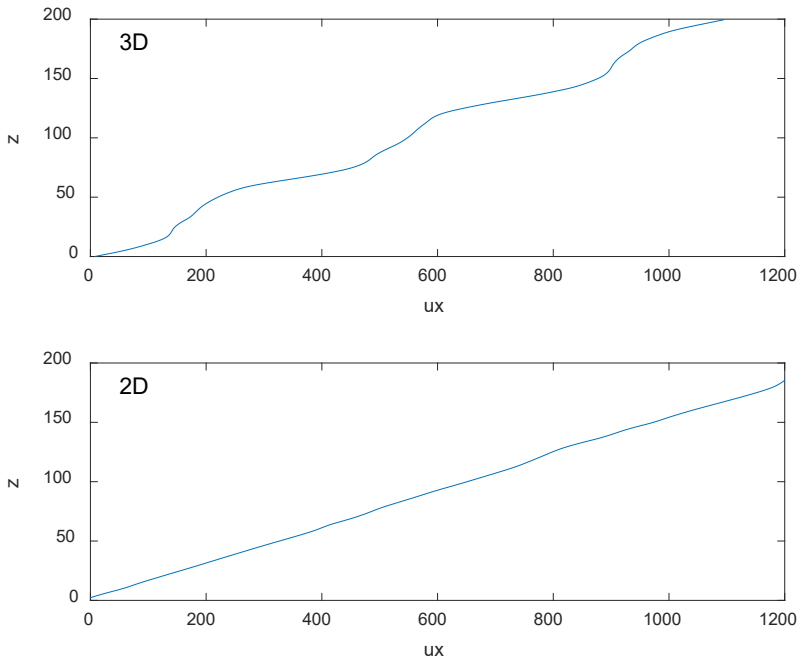

Figure 8. 3D vs 2D Shear Profiles

We also conduct a full steppiness evaluation for the 9 2D simulations, displayed in Figure 9. All 9 simulations show a similar pattern. As in 3D, higher density ratios $(R_0 = 5)$ reach a uniform density gradient much sooner than lower density ratios $(R_0 = 3, R_0 = 2)$ even though the process by which the simulation transitions to this stage is markedly

different. It is also possible to correlate the 2D staircase destruction process in Figure 7 with the steppiness parameters in Figure 9. The initial development of shear-induced turbulence is seen in the beginning of all 9 simulations in Figure 9, where the steppiness value begins to decrease quickly. This is representative of the first stage in Figure 7a, where turbulence begins to mix the layers. However, the steppiness values in Figure 9 then begin to increase as the shear begins to stabilize the interfaces. This stage is correlated to Figure 7b, where convection is fully realized but begins to decrease as shear increases. Finally, the continually increasing shear effectively shuts down convection leaving only molecular diffusion to continue mixing the layers, as seen in Figure 7c. In Figure 9, the steppiness parameter decreases slowly at late times in every simulation as salt diffuses the remnants of the staircase.

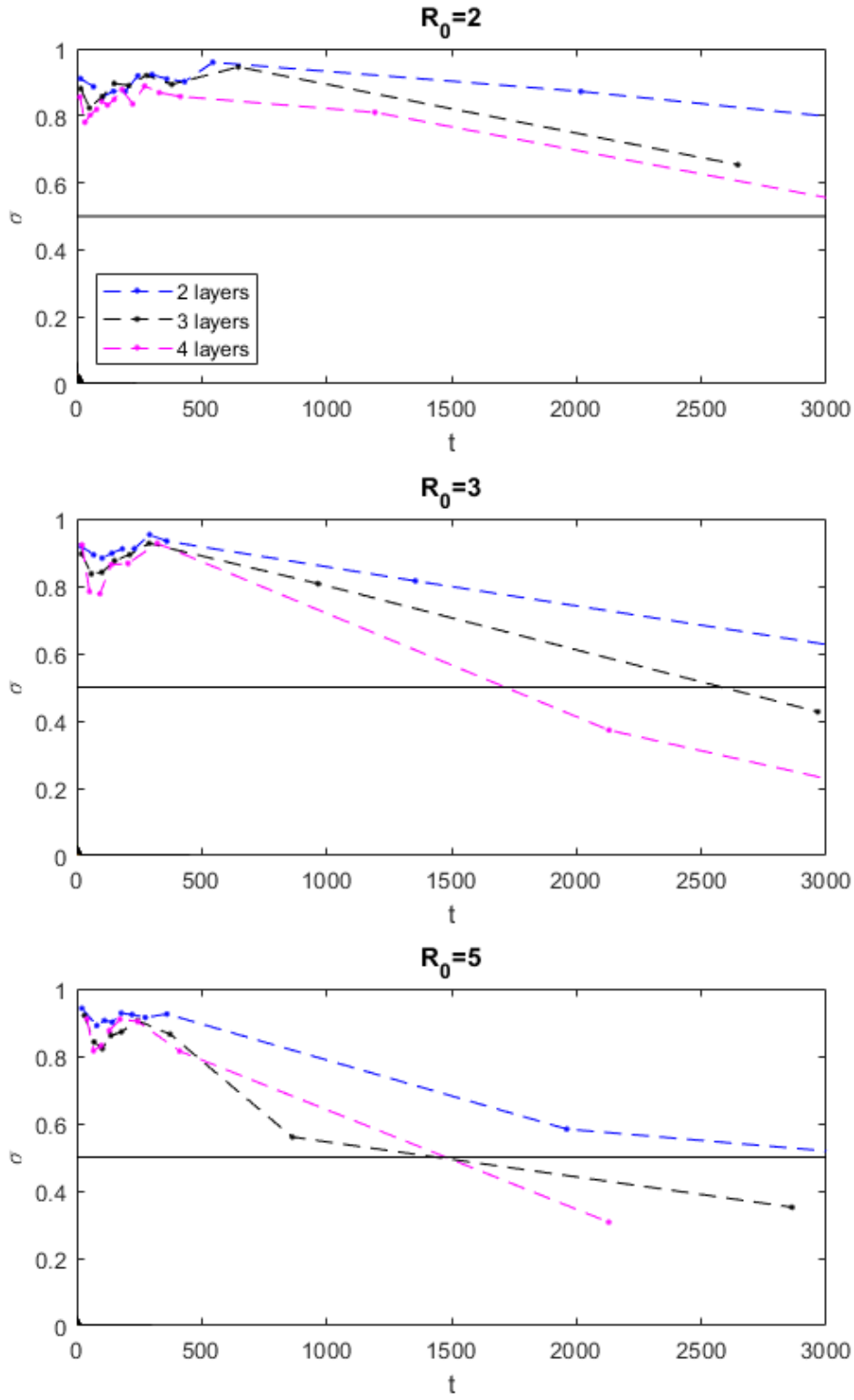

Figure 9. Steppiness (σ) Parameters for 2D Simulations

THIS PAGE INTENTIONALLY LEFT BLANK

IV. STAIRCASE FORMATION

We also model staircase creation via shear instabilities in order to fully describe the life cycle of thermohaline staircases in the presence of shear. We simulated two cases with different Richardson numbers in a square box of side length $L = 100$ resolved by 3072 grid points in each dimension. Both simulations had $\mathrm{Pr} = 10$, $\tau = 0.01$, $R_0 = 2$, and $\omega = 0.3$. However, the $\mathrm{Ri} = 2$ simulation had $\gamma_r = 0$ and $\gamma_0 = \sqrt{10}$ while the other (Ri = 3) had $\gamma_r = 0$ and $\gamma_0 = \sqrt{\frac{20}{3}}$. Each simulation began with uniform gradients of temperature, salinity, and velocity, and the temperature and salinity were seeded with small random perturbations.

Figure 10 shows a series of density perturbation snapshots of the $\mathrm{Ri} = 3$ simulation. Figure 10a shows the initial instability that takes the form of plane waves in the sheared coordinate system. This comes from the nature of the fluid equations: at early times, the perturbations are small, and so the nonlinear terms (which are quadratic) are negligible, resulting in a linear set of equations for which plane waves are the solution. The growth rate of these plane waves depends on the wavenumbers, and typically one of these grows fastest of the simulated modes. As the perturbation amplitudes increase, and the nonlinear terms are no longer negligible, Figure 10b shows the introduction of larger non-linearities and turbulence, as well as the development of nascent layer-like structures, likely caused by the growth of the instability eventually leading to small-scale wave breaking. Next, Figure 10c shows that the small, sharp features have continued to merge over time into strongly horizontal layers across the parameter space, as is typical of DDC. At this stage, the thermohaline–shear instability has served an analogous function to diffusive convection, which is known to generate layers (Radko, 2013) but has done so outside of the parameters typically unstable to DDC. Finally, Figure 10d highlights how layers merge by entraining material into adjacent layers, shifting the height of the interface until one of the layers has been completely entrained. Radko (2013) shows that this layer merging phenomenon is relatively common for this type of simulation and that eventually, these

simulations could have both continued to merge into one single resultant layer. However, the time it takes for layers to merge becomes progressively longer and computationally taxing, so the simulations were terminated early.

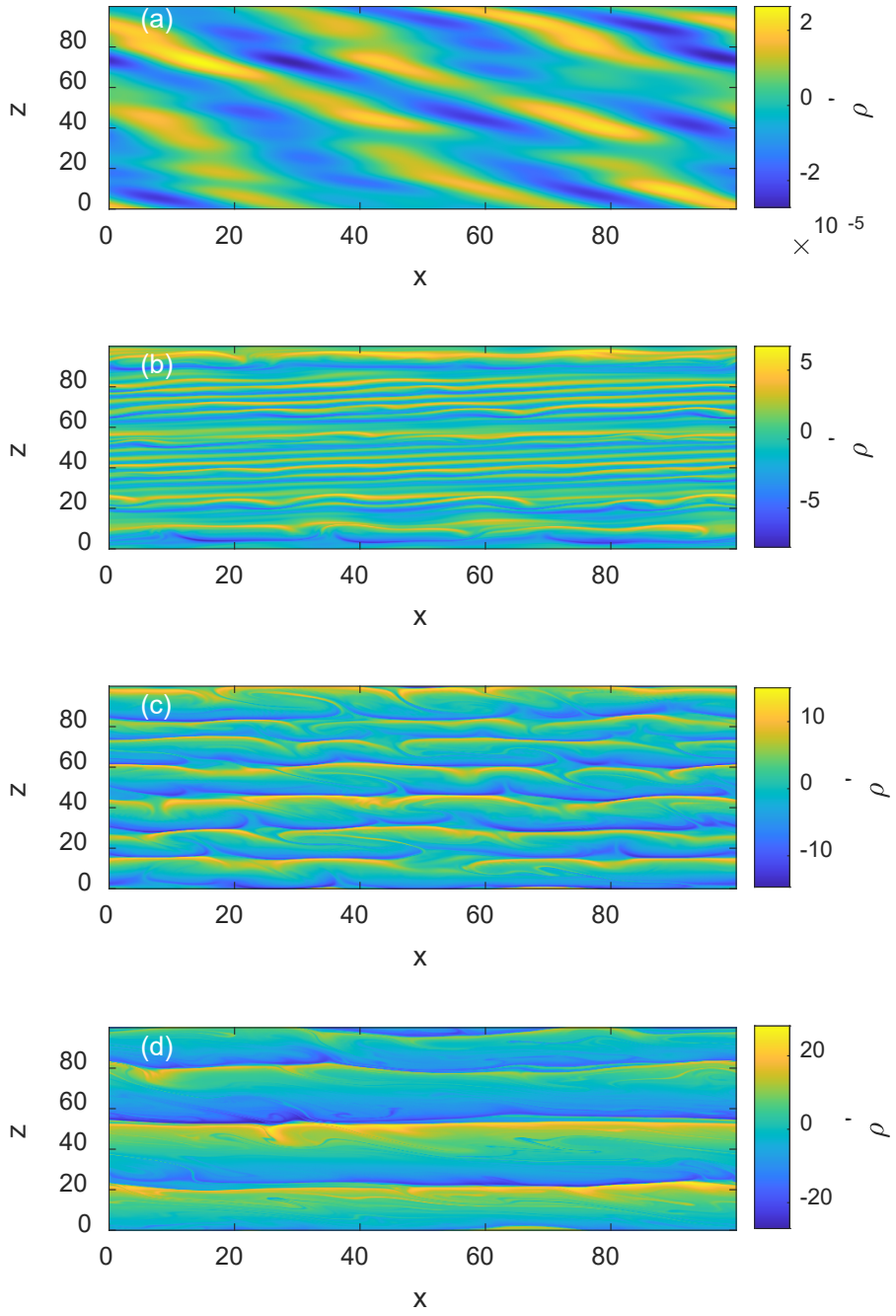

Figure 10. Density Perturbations Leading to Staircase Formation for Ri = 3

We conducted a heat flux analysis for both staircase-building simulations in Figure 11. Initially ($t < 1000$, $t < 1500$ for Ri=2, Ri=3, respectively), there are small instabilities

that arise from the application of shear that slowly grow over time. Notably, the case with Ri=2 has a higher growth rate than the one with Ri=3, which is consistent with linear stability analyses (see Radko, 2016). Eventually, the heat flux reaches a relative equilibrium once the staircase is formed. We can further analyze this equilibrium by observing the steppiness parameter for both simulations.

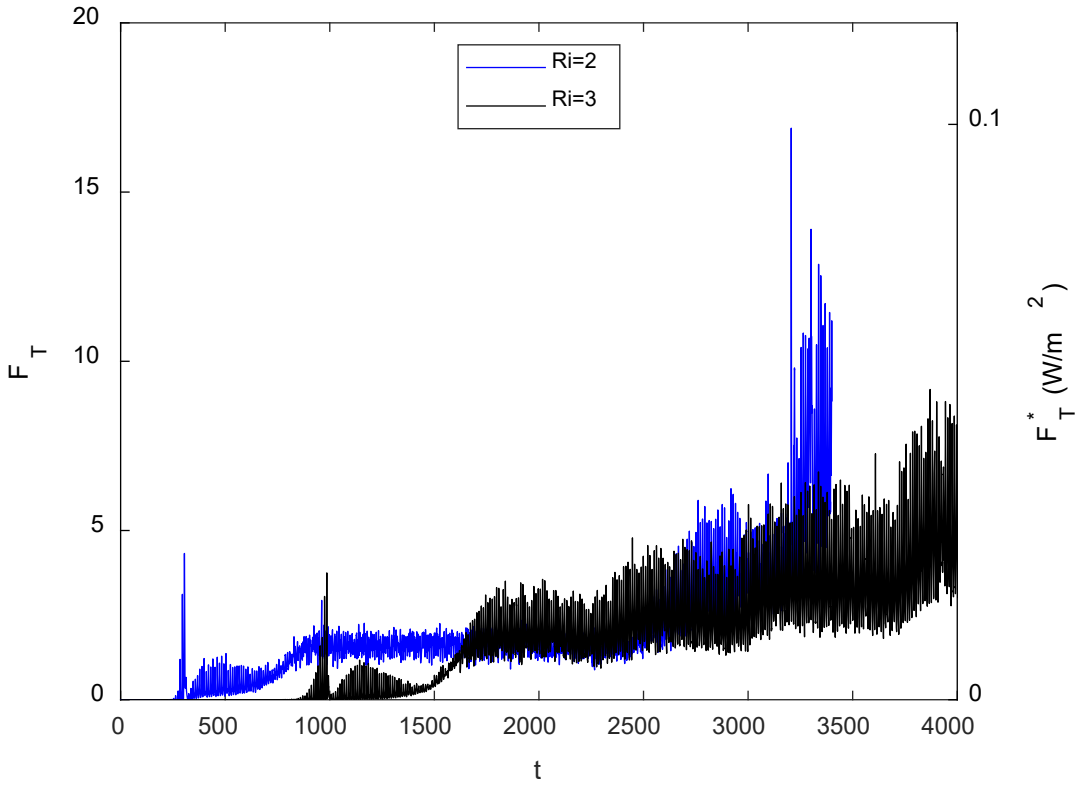

Figure 11. Heat Fluxes for Staircase Formation Simulations

The steppiness results of both simulations are displayed in Figure 12. For these, the steppiness begins at 0, indicating a perfectly uniform density gradient. As the turbulence increases and layers begin to form, the steppiness parameter crosses the $\sigma = 0.5$ threshold. Notably, the Ri=2 simulation crosses that threshold before the Ri=3 simulation does due to the higher thermohaline–shear instability growth rate. The steppiness parameter for the case with Ri=2 indicates that the staircase is present at about $t = 600$. However, Figure 11 shows that heat flux is still increasing until roughly $t = 1000$, indicating that the staircase

has not reached a heat flux equilibrium. Similarly, the staircase is present in Figure 12 for Ri=3 at about $t = 1500$ while heat flux begins to plateau in Figure 11 at about $t = 1600$. This indicates that the production of staircase-like structures precedes the thermal equilibrium of the system, and so the structure of the staircase must likely adjust for the first few hundred non-dimensional time units.

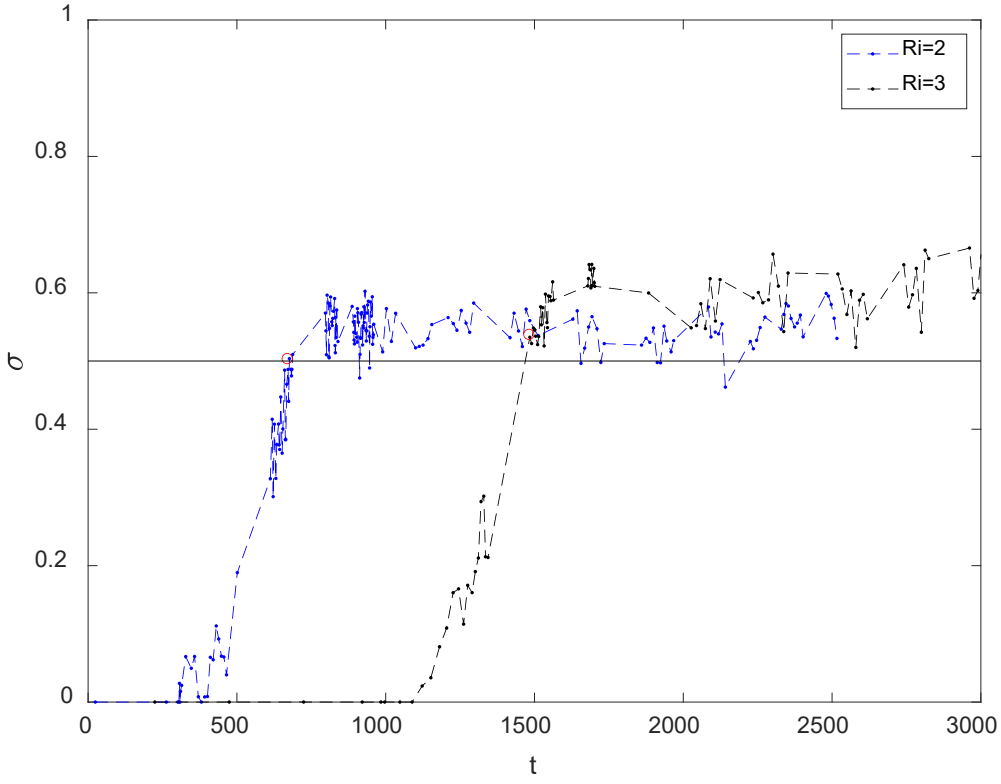

Figure 12. Steppiness (σ) Values for 2D Simulations

THIS PAGE INTENTIONALLY LEFT BLANK

V. CONCLUSIONS

Double diffusive convection is indeed a fascinating subject with significant implications for Arctic heat fluxes as well as World Ocean circulation. In this study, we modeled the effects of internal wave-driven vertical shear on the formation and destruction of thermohaline staircases. We found via direct numerical simulation that shear does contribute to the disruption of staircases when its strength approaches the level required for the Kelvin–Helmholtz instability. We also found that higher density ratios are disrupted with less shear than lower density ratios. We found no significant differences in critical Richardson numbers in simulations with unidirectional shear as compared to those with multidirectional shear. However, there are significant differences in heat flux signatures between the two. Finally, we found that 2D simulations with shear do not accurately represent staircase destruction.

Furthermore, we also modeled that relatively weak shear (significantly outside the threshold of Kelvin–Helmholtz instability) can generate layers in a thermohaline staircase. We found in these simulations that layers start at small vertical extents and continue to merge over time by entraining adjacent layers. Staircase formation does depend on Richardson number, where lower Richardson numbers form staircases more quickly than higher Richardson numbers. Also, “H” type mergers were prevalent in shear-induced staircase formation simulations (Radko et al., 2014).

We also established a steppiness parameter to quantify the existence of a staircase. The steppiness of a staircase is calculated from the distribution of density in the simulated domain and identifies large regions of nearly uniform density. This parameter can be used to evaluate both the destruction and formation of thermohaline staircases, and it agrees reasonably with visual inspection. This development could provide a useful tool for investigating the presence and sharpness of staircases in both numerical and observational work with a consistent algorithm.

Indeed, the Arctic is undoubtedly becoming of greater interest to the United States Navy with the looming implications of global climate change. It is critical to understand

Arctic heat flux as the rate of ice melt continues to increase, and the Arctic becomes more and more accessible. Because thermohaline staircases are nearly ubiquitous in the Arctic thermocline, the flux transport in these systems is important to understand in order to accurately parameterize the heat transport from the warmer Atlantic Water to the Arctic surface. It is critical to understand the conditions conducive (or not conducive) to thermohaline staircases in order to fully understand and evaluate Arctic heat transport.

Thermohaline staircases also have acoustic implications relevant to the United States Navy. Acoustic transmission in seawater is affected by temperature, salinity, and density. When all three ingredients are packed into a staircase structure, the resultant sound velocity profile is also stepped. These layers in sound speed can trap and duct sound for extremely long ranges, increasing the range of acoustic detection. However, more research is required to fully understand the implications of operating in areas of thermohaline staircases.

There are several other opportunities to expand upon this research. First, the steppiness parameter could be evaluated for actual CTD measurements of thermohaline staircases. This would permit the capacity to compare the bulk parameters of observed staircases against simulations and to quantify local variations in staircase structure. Furthermore, this study could be replicated with constant shear vice increasing shear. In that situation, constant levels of shear could be simulated until staircase destruction and compared across Richardson numbers. Finally, a more thorough study of 3D staircase formation in the presence of weak shear would provide more insight to the overall role of shear in thermohaline staircases.

LIST OF REFERENCES

Bebieva, Y., & Timmermans, M.-L. (2017). The relationship between double-diffusive intrusions and staircases in the Arctic Ocean. *Journal of Physical Oceanography*, *47*(4), 867–878. https://doi.org/10.1175/JPO-D-16-0265.1

Canuto, C., Hussaini, M. Y., Quarteroni, A., & Zang, T. A. (2007). *Spectral methods: Evolution to complex geometries and applications to fluid dynamics*. Springer-Verlag. https://doi.org/10.1007/978-3-540-30728-0

Flanagan, J. D., Lefler, A. S., & Radko, T. (2013). Heat transport through diffusive interfaces. *Geophysical Research Letters*, *40*(10), 2466–2470. https://doi.org/10.1002/grl.50440

Jevons, W. S. (1857). II. On the cirrous form of cloud. *The London, Edinburgh and Dublin Philosophical Magazine and Journal of Science*, *14*(90), 22–35. https://doi.org/10.1080/14786445708642347

Kwok, R., & Untersteiner, N. (2011). The thinning of Arctic sea ice. *Physics Today*, *64*(4), 36–41. https://doi.org/10.1063/1.3580491

Lipps, F. B. (1971). Two-dimensional numerical experiments in thermal convection with vertical shear. *Journal of the Atmospheric Sciences*, *28*(1), 3–19. https://doi.org/10.1175/1520-0469(1971)028<0003:TDNEIT>2.0.CO;2

Molemaker, M. J., & Dijkstrad, H. A. (1997). The formation and evolution of a diffusive interface. *Journal of Fluid Mechanics*, *331*, 199–229. https://doi.org/10.1017/S0022112096003862

Neal, V. T., Neshyba, S., & Denner, W. (1969). Thermal stratification in the Arctic Ocean. *Science*, *166*(3903), 373–374.

Orszag, S. A., & Patterson, G. S. (1972). Numerical simulation of three-dimensional homogeneous isotropic turbulence. *Physical Review Letters*, *28*(2), 76–79. https://doi.org/10.1103/PhysRevLett.28.76

Radko, T., Flanagan, J. D., Stellmach, S., & Timmermans, M.-L. (2014). Double-diffusive recipes. Part II: Layer-merging events. *Journal of Physical Oceanography*, *44*(5), 1285–1305. https://doi.org/10.1175/JPO-D-13-0156.1

Radko, Timour. (2013). *Double-diffusive convection*. University Press.

Radko, Timour. (2016). Thermohaline layering in dynamically and diffusively stable shear flows. *Journal of Fluid Mechanics*, *805*, 147–170. https://doi.org/10.1017/jfm.2016.547

Shibley, N. C., Timmermans, M.-L., Carpenter, J. R., & Toole, J. M. (2017). Spatial variability of the Arctic Ocean's double-diffusive staircase. *Journal of Geophysical Research: Oceans*, *122*(2), 980–994. https://doi.org/10.1002/2016JC012419

Smyth, W. D., & Kimura, S. (2007). Instability and diapycnal momentum transport in a double-diffusive, stratified shear layer. *Journal of Physical Oceanography*, *37*(6), 1551–1565. https://doi.org/10.1175/JPO3070.1

Stern, M. E. (1960). The "salt-fountain" and thermohaline convection. *Tellus*, *12*(2), 172–175. https://doi.org/10.1111/j.2153-3490.1960.tb01295.x

Traxler, A., Stellmach, S., Garaud, P., Radko, T., & Brummell, N. (2011). Dynamics of fingering convection. Part 1 small-scale fluxes and large-scale instabilities. *Journal of Fluid Mechanics*, *677*, 530–553. https://doi.org/10.1017/jfm.2011.98

Turner, J. S. (1965). The coupled turbulent transports of salt and heat across a sharp density interface. *International Journal of Heat and Mass Transfer*, *8*(5), 759–767. https://doi.org/10.1016/0017-9310(65)90022-0

Turner, J. S. (2010). The melting of ice in the Arctic Ocean: The influence of double-diffusive transport of heat from below. *Journal of Physical Oceanography*, *40*(1), 249–256. https://doi.org/10.1175/2009JPO4279.1

Turner, J. S., & Stommel, H. (1964). A new case of convection in the presence of combined vertical salinity and temperature gradients. *Proceedings of the National Academy of Sciences - PNAS*, *52*(1), 49–53. https://doi.org/10.1073/pnas.52.1.49

INITIAL DISTRIBUTION LIST

1. Defense Technical Information Center
   Ft. Belvoir, Virginia

2. Dudley Knox Library
   Naval Postgraduate School
   Monterey, California